

PL-001

Crystal structure of Photosystem II and aspects of its function

HT Witt¹, A Zouni¹, J Kern¹, P Fromme¹, N Krauß², W Saenger² and P Orth²

¹*Max-Volmer-Laboratorium für Biophysikalische Chemie und Biochemie, Technische Universität Berlin, Str. d. 17. Juni 135, 10623 Berlin, Germany*

²*Institut für Chemie/Kristallographie, Freie Universität Berlin, Takustr. 6, 14195 Berlin, Germany*

Keywords: photosystem II, crystal structure, electron transfer, manganese cluster

Abstract A short description of the X-ray structure of photosystem II at 3.8 Å resolution is presented. Following these results, functional aspects are discussed.

Introduction

In water-oxidizing photosynthesis two photosystems (PS I and PS II) operate in series. These large pigment-protein complexes are integrated into the thylakoid membrane. Following light excitation, finally electrons are transferred from water to the terminal electron acceptor NADP. The water oxidation in PS II supplies the overall process with the necessary electrons and protons and the atmosphere with oxygen. This process starts with a transmembrane ejection of an electron from the excited primary electron donor, chlorophyll P680, at the luminal membrane side, via a pheophytin, to the electron-stabilizing acceptor, a plastoquinone, Q_A, at the stromal side. For oxidation of 2 H₂O the created univalent radical of P680 abstracts, via a tyrosine Y_Z, in four successive charge-separating steps, four electrons from the water-oxidizing manganese cluster coupled with the release of four protons and the evolution of one O₂ at the luminal side. The protons contribute to the electrochemical gradient that drives ATP synthesis (for a review see (Witt, 1996)). Structural information on the architecture of PS II has been obtained by electron microscopy at 10-30 Å resolution (Nield et al., 2000) and by electron crystallography on 2D crystals of PS II fragments without the water-oxidizing apparatus at 8 Å resolution (Rhee et al., 1998). Here, we discuss – based on the X-ray structure of PS II at 3.8 Å resolution of 3D crystals capable of water cleavage (Zouni et al., 2001) – also aspects of its function.

Structure

PS II was isolated from the membranes of the thermophilic cyanobacterium *Synechococcus elongatus* and crystallized (Zouni et al., 1998). By measurement of H⁺- and O₂-release from the illuminated crystals themselves, it was shown that they have not lost their capability for water oxidation by the crystallization procedure (Zouni et al., 2000). The structure of the PSII dimer was obtained at 3.8 Å resolution using X-rays from a synchrotron radiation source at cryogenic temperature (100K).

The electron density obtained by multiple isomorphous replacement indicates a field of 36 transmembrane α -helices and 39 cofactors per PS II monomer. Two groups of 5

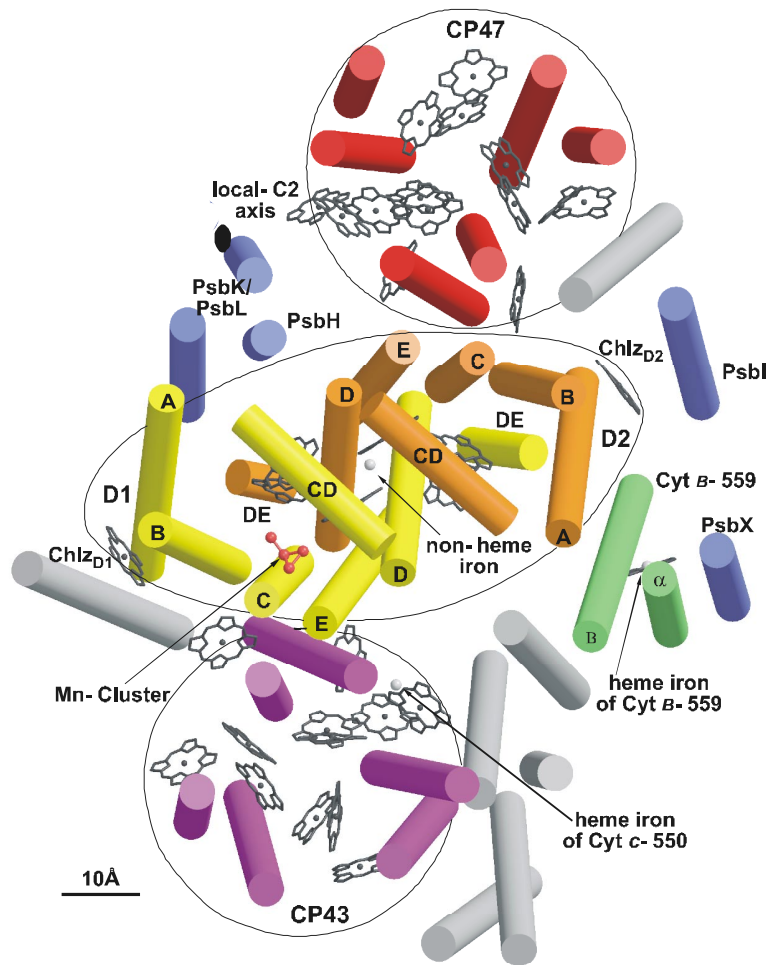


Fig. 1: Arrangement of the α -helices and cofactors in one monomer of the PS II core complex. View direction from the luminal side onto the membrane plane (Zouni et al, 2001 modified).

transmembrane α -helices each are arranged in two semicircles interlocked in a hand shake-like motif and related by a pseudo-C2 axis. They have been assigned to α -helices A to E of the subunits D1 and D2, respectively (Fig. 1). The arrangement of these five α -helices of D1 and D2 resembles that of subunits L and M in the purple bacterial reaction center (PbRC) (Michel and Deisenhofer, 1988) and the 5C-terminal helices of PsaA and PsaB in photosystem I (Schubert et al., 1998). Six α -helices are arranged as trimer of dimers related by the pseudo-C2 axis and coordinate the antenna Chl *a* in CP43 and CP47. They contain 12 and 14 Chl *a*, respectively. The molecules are arranged in two layers close to the stromal and luminal membrane side. One Cyt b-559, with its two subunits α and β each forming a transmembrane α -helix, has been identified by the high electron density of its heme iron. Two helices close to D2 and Cyt b-559 were putatively assigned to PsbI and PsbX. PsbH, PsbK and PsbL have been implicated in the stabilization of the PS II dimer. They were tentatively assigned to a 3-helix bundle close to the local C2 axis. Seven additional transmembrane α -helices (grey α -helices) could not be assigned. Three maxima of the electron density were assigned to iron and one more extended to the Mn cluster at about 15 Å apart from the pseudo-C2 axis (Fig. 1).

At the luminal side of the electron density, two of the three extrinsic subunits (Cyt c-550, 33 kDa protein, and 12 kDa protein) could be located unambiguously (Figs. 2). The position of Cyt c-550 is indicated by its heme iron, surrounded by three tubular structures. A ~ 35 Å long, cylindrical arrangement characterized by β -strands with yet uncertain connectivities has been assigned to the Mn-stabilizing 33 kDa subunit (PsbO); it is tilted against the membrane by 45° and corresponds to about half of the molecular mass of this subunit. The expected extrinsic 12 kDa subunit could not yet be located because of its vicinity to unassigned structure elements and long loops of D1, D2, CP43 and CP47.

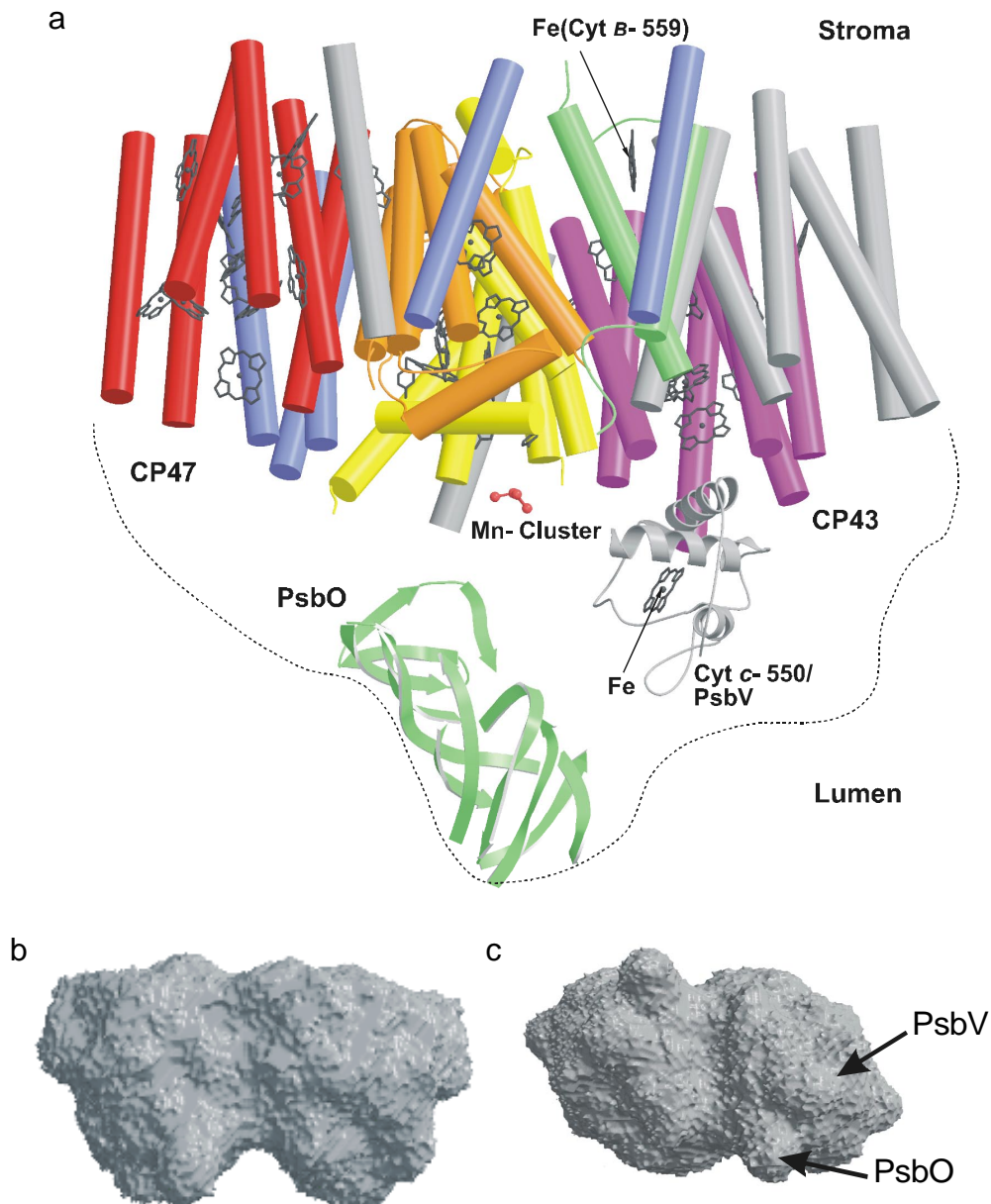


Fig. 2: (a) Side view of the monomer in Fig. 1 down the long axis of the D2-D1 subunit at slightly tilted membrane plane (Zouni et al, 2001). (b) Surface of the PSII homodimer, view along the membrane plane, (c) view onto the membrane from the luminal side. The location of the subunits PsbO and PsbV are visible by their prominent bulges.

The cofactors of the electron transfer chain (ETC), suspended between subunit D1 and D2, form two branches organized symmetrically along the pseudo-C2 axis (Fig. 3). Towards the luminal side, two Chl *a* molecules (P_{D1} and P_{D2}) are observed, assigned to P680. Towards the stromal side, two Chl *a* (Chl_{D1} and Chl_{D2}) are located at 9.8 and 10 Å, respectively, apart from P_{D1} and P_{D2}. Their planes are tilted ~30° against the membrane plane, analogous to the accessory bacteriochlorophylls in PbRC. They are followed by Pheo_{D1} and Pheo_{D2}. The site of tightly bound plastoquinone, Q_A, is at 12 Å from Pheo_{D1} and at 10.5 Å distance from the non-heme iron. The putative docking site for the mobile Q_B is not occupied.

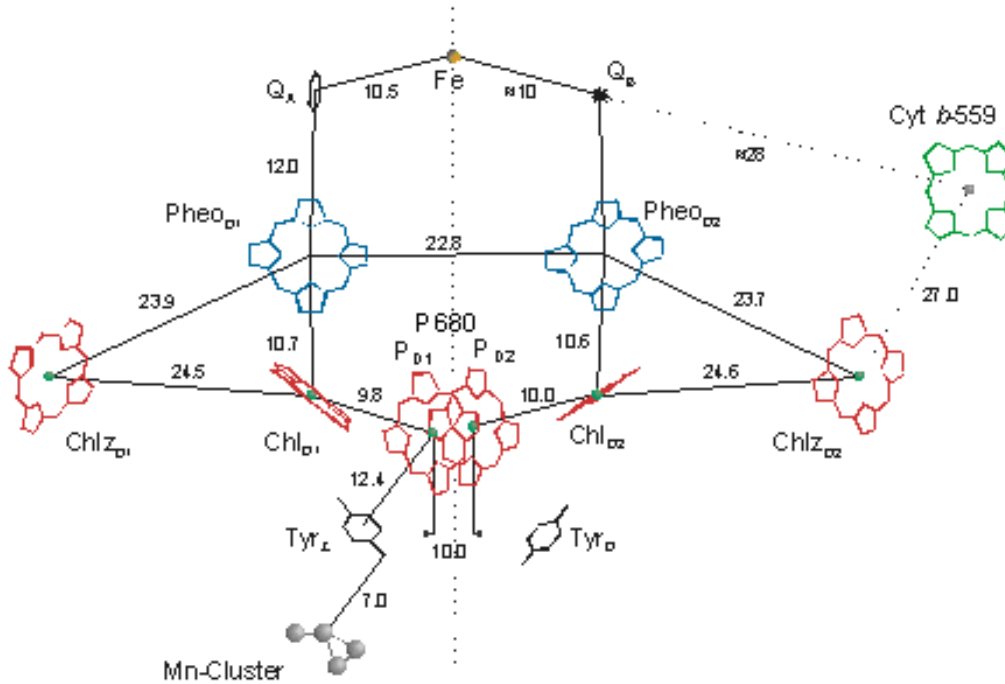


Fig. 3: Arrangement of cofactors of the electron transfer chain in subunits D1 and D2. View direction along the membrane plane. The center-to-center distances (Å) are indicated. The pseudo-C2 axis is shown by the vertical dotted line (Zouni et al. 2001, modified).

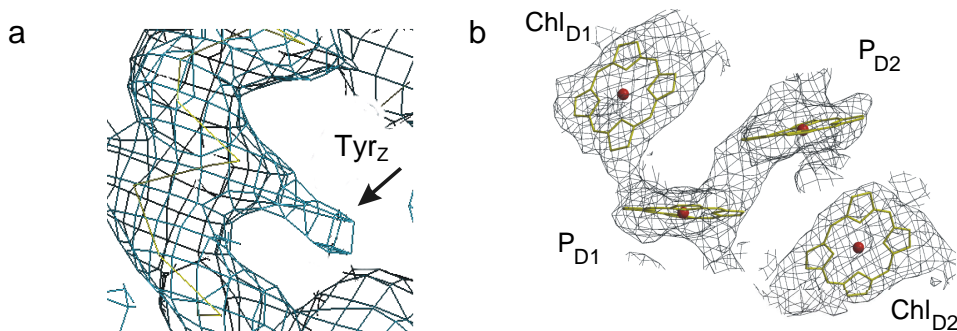


Fig. 4: (a) Electron density of the tyrosine side chain 161 of D1 (see arrow). (b) Electron density contoured around P680 and the Chl_{D1,D2} at 1.3 σ (root mean square deviation above the mean electron density). View from the luminal side onto the membrane.

Two extra Chl *a* on the periphery of D1 and D2 named Chl_{D1} and Chl_{D2} are possibly functioning as a link for the exciton transfer from the antenna systems to the core of the reaction center (see also Fig. 1). The pseudo-C2 symmetry of the cofactor arrangement is broken by Cyt b-559 and the Mn cluster. The electron transfer chain between P_{D1} and the Mn cluster is bridged by the redox-active tyrosine 161 of D1 (Tyr_Z). The latter could be located through a protrusion of the electron density in the last turn at the luminal side of helix C in D1 (Fig. 4a). Tyrosine 161 of D2 (Tyr_D) was found at a corresponding position at helix C in D2. Fig. 4b shows that the head groups of P_{D1} and P_{D2} are parallel (with 5 Å interplanar distance) and arranged perpendicular to the membrane plane (center-to-center distance 10 Å). Due to the large distance between these two chlorophylls, excitonic coupling is weak and they can be regarded as monomeric chlorophylls. The cationic radical of P680 is very probably located on P_{D1} which is close to Tyr_Z as this acts as an immediate electron donor to the cationic radical.

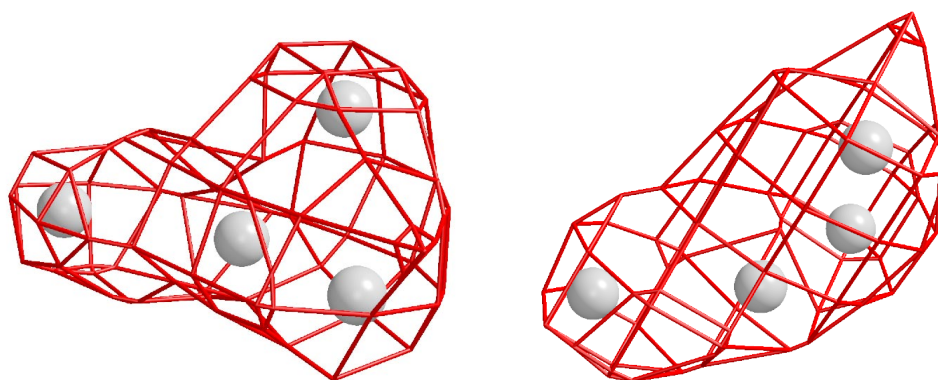


Fig. 5: Electron density of the Mn cluster contoured at 5 σ . View from the luminal side onto the membrane plane (left). View along the membrane with the luminal side on top (right) (Zouni et al. 2001, modified).

The electron density assigned to the Mn cluster in Fig. 5 is bulged in three directions in the form of a "Y". The dimensions of the electron density are 6.8 Å x 4.9 Å x 3.3 Å; the long axis in Fig. 5, right, is tilted $\sim 23^\circ$ against the membrane plane. The three bulges of the electron density were assigned to the density of 3 Mn ions and the density near the center to a fourth Mn ion. The inter-atomic distances are about 3 Å. To verify that the electron density of this cluster is due to the contribution of manganese, anomalous diffraction data were collected with X-ray wavelength close to the Mn edge (1.894 Å). The global maximum of an electron density calculated with these data matches quite well the model shown in Fig. 5.

Functional aspects

At the present resolution of 3.8 Å it is not possible to use the Mn-model for discussing the likely functional mechanism of water oxidation. Crystals of higher quality are therefore in preparation. However, the contoured electron density in Fig. 5 can be used for a comparison with numerous published models presented as possible candidates for water oxidation. A great part of them can thereby be clearly excluded; only a very few

remain for a closer inspection. Beside Mn ions, Ca^{2+} ions are important for water oxidation. They could not be located. In order to make their position nevertheless visible at the present resolution, Ca^{2+} ions have to be exchanged at their catalytic site against ions with higher electron density. This work is in progress.

With respect to the ETC shown in Fig. 3, which drives the water oxidation, this is at first glance – in spite of the outstanding high oxidation potential of P680 and the therefore expected structural peculiarity – not very different from the ETC of PS I and PbRC (Schubert et al., 1998; Michel and Deisenhofer, 1988): (1) the scaffolding of the 10 helices between which the ETC is suspended, is similar in all three types of RC; (2) the basic constructions of the two branches of the cofactors are also comparable in these three systems; (3) the assembly of the primary donors in each of these systems consists of a pair of chlorophylls. However, a closer inspection shows properties of PS II being essentially different from PS I and PbRC.

The center-to-center distance of the Chl pair of P680 is 10 Å. This is large and, therefore, $\text{P}_{\text{D}1}$ and $\text{P}_{\text{D}2}$ may be regarded as monomers. This is a striking difference compared with the primary donors of PS I and PbRC, where the chlorophylls are in close contact and have been identified as dimers. The other porphyrins of the ETC in PS II are also ca. 10 Å apart from each other. Thus we can regard these cofactors as an ensemble of 6 weakly coupled monomeric porphyrins. This feature has consequences with respect to conclusions about the redox potentials of the cofactors as well as the nature of the primary donor.

Pheo has an oxidation potential E_{m} of ~1.4 V, the cationic radical of P680 ($\text{P}_{\text{D}1}^+$; see above) is expected to have ≥ 1.1 V in order to be capable of water oxidation. However, monomeric Chls *in vitro* have a maximum of ~0.8 V and probably also the antenna Chls *in vivo*. In the latter case the cationic radical, $\text{P}_{\text{D}1}^+$, would oxidize the nearby monomeric $\text{Chl}_{\text{D}1}$ instead of Tyr_Z (~1.0 V). Therefore, in some previous publications on the possible arrangement of these porphyrins, the location of a Chl between $\text{P}_{\text{D}1}$ and $\text{Pheo}_{\text{D}1}$ had been excluded. However, our structural results now indicate the presence of $\text{Chl}_{\text{D}1}$ at this position. From this follows the important conclusion that the oxidation potential of $\text{Chl}_{\text{D}1}$ must be higher than that of $\text{P}_{\text{D}1}$ e.g. 1.3 V. This must also be the case for the neighboring $\text{P}_{\text{D}2}$. If so, $\text{Chl}_{\text{D}1}$ and $\text{P}_{\text{D}2}$ are resistant to oxidation by $\text{P}_{\text{D}1}^+$. In this way the charge separation is stabilized and $\text{P}_{\text{D}1}^+$ is capable of oxidizing Tyr_Z.

Following this conclusion, the considered high oxidation potential of $\text{Chl}_{\text{D}1}$ raises the question as to why $\text{Chl}_{\text{D}1}$ itself is not the primary electron donor and the cationic radical state $\text{Chl}_{\text{D}1}^+$ the driving force for water oxidation. Due to the weak coupling of the porphyrins, there is almost no spectral separation between them (this is in contrast to the strong coupling in PbRC). Thus, in PS II, the absorption bands are largely overlapping and centered between 670-680 nm. The antenna system can therefore provide each of the porphyrins with excitation energy followed by energy transfer between them. If $\text{Chl}_{\text{D}1}$ has a ground state absorption spectrum at clearly lower energy than $\text{P}_{\text{D}1}$, the energy is primarily trapped by $\text{Chl}_{\text{D}1}$ provided that energy equilibration within the pigments is much faster than charge separation. In this case, the excited $\text{Chl}_{\text{D}1}$ can operate as primary electron donor, reducing $\text{Pheo}_{\text{D}1}$ and $\text{Chl}_{\text{D}1}^+$ subsequently oxidizes

P_{D1} . Here, P_{D1} is functioning as an intermediate electron donor for Chl_{D1}^+ . Independent of these two different scenarios for primary electron donation, the cationic radical, which oxidizes Tyr_Z , is in both cases the P_{D1}^+ chlorophyll.

Experimental support that Chl_{D1} is indeed the species that has a longer wavelength absorption than P_{D1} is given by measurements at low temperature. The spectrum of the flash-induced redox reaction of PS II is characterized by a maximum bleaching at 673 nm and one at 683 nm at 80 K (Hillmann et al., 1995; Diner et al., 2001). Mutation of the His 198 residue, which coordinates the Mg^{2+} of P_{D1} , indicates that $\lambda_{max} \approx 673$ nm is correlated with the absorption spectrum of P_{D1} (Fig.6) (the absorption of the P_{D1} cation is negligible around 673 nm). The bleaching at 683 nm does not respond at ≤ 80 K to the mutation and must belong to the spectral feature of a different component. The negative change at 683 nm is associated with a positive change at 678 nm. This is explained by an electrochromic blue-shift induced by the charge of P_{D1}^+ on the absorption band of a neighboring Chl, if this is centered at $\lambda_{max} \approx 681$ nm (Diner et al., 2001). Following the above discussion, this band must represent the spectrum of Chl_{D1} (Fig. 6). According to the Boltzmann distribution and the energy gap of ~ 30 meV between P_{D1} (673 nm) and Chl_{D1} (681 nm), the primary charge separation may be driven at low temperature (≤ 80 K) only by Chl_{D1}^* . At higher temperatures, P_{D1}^* will increasingly participate in this process up to ca 20 % at room temperature if the gap remains constant. But recently a decrease of the gap with increasing temperature was observed (private communication by E. Schlodder). Therefore the contribution of P_{D1}^* is >20 % at room temperature and maximal 50 % if the gap would be close to zero.

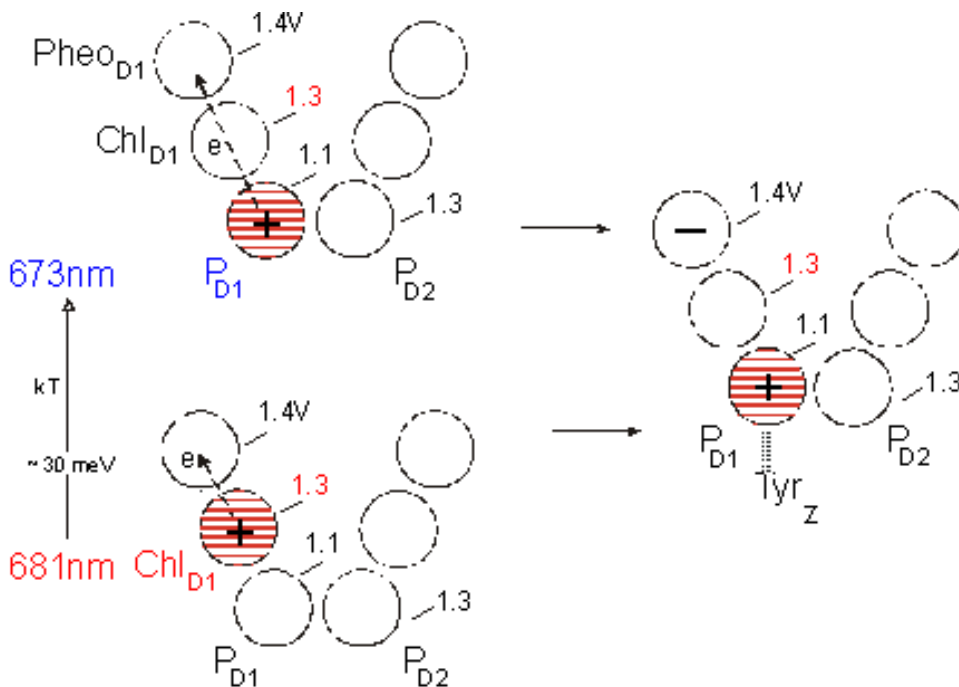


Fig. 6: Simplified scheme of the six „monomeric“ porphyrins of the ETC with P_{D1} and Chl_{D1} acting as primary electron donors (details see text).

Independent evidence that Chl_{D1} acts as the primary electron donor at low temperature is based on the fact that the Chl-triplet state in the RC of PS II - which is assumed to be on the same Chl as the primary donor - has been observed to be located on a monomeric Chl tilted by 30° against the membrane plane (Mieghem et al., 1991). But, this is exactly the orientation of Chl_{D1} determined by the X-ray structure shown in Fig. 3.

Regardless of these perspectives, we are left with the question of how the unique high redox potential of P_{D1} is established as well as the possible, even higher ones of Chl_{D1} and P_{D2}. Hydrogen bonding between carbonyl groups of the porphyrins and protons of amino acid residues of nearby helices may be an essential factor for the rise of the redox potential. It was shown for BChl that in this way the gain can be 60-100 mV per bond (Allen and Williams, 1995). A further increase of the potential could be achieved by the electrostatic influence of positively charged residues in the neighborhood of the porphyrins (Mulkiđjanian, 1999). A contribution maximum of such a charge is expected when this is in the immediate vicinity of the chlorophylls. In a Schiff-base chlorophyll it was shown that by its protonation the redox potential is increased by 310 mV (Maggiara et al., 1985). Obviously, evolution has realized the tuning of high potentials, not by fascinating new constructions but by very tiny changes in the microenvironment – perhaps even only by a protonation at the right place.

Acknowledgements

We would like to thank E. Schlodder (Max-Volmer-Institut, Berlin) for helpful discussion and for providing us the Diner et al. reference before publication

References

- Allen JP, Williams, JC (1995) Relationship between the oxidation potential of the bacteriochlorophyll dimer and electron transfer in photosynthetic reaction centers. *J. Bioenergetics and Biomembranes* **27**, .
- Diner BA, Schlodder E, Nixon PJ, Coleman WJ, Rappaport F, Lavergne J, Vermaas WFJ, Chisholm DA (2001) Site-directed mutations at D1-His198 and D2-His197 of photosystem II in *Synechocystis* 6803: Sites of primary charge separation and cation and triplet stabilization. *Biochemistry*, in press
- Hillmann B, Brettel K, van Mieghem F, Kamłowski A, Rutherford AW, Schlodder E (1995) Charge recombination reactions in photosystem II. 2. Transient absorbance difference spectra and their temperature dependence. *Biochemistry* **84**, 4814-4827.
- Maggiara LL, Petke JD, Gopal D, Iwamoto RT, Maggiara GM (1985) Experimental and theoretical studies of Schiff base chlorophylls. *Photochem. Photobiol.* **42**, 69-75.
- Michel H, Deisenhofer, J (1988) Relevance of the photosynthetic reaction center from purple bacteria to the structure of photosystem II. *Biochemistry* **22**, 1-7.
- Mulkiđjanian AY (1999) Photosystem II of green plants: On the possible role of retarded protonic relaxation in water oxidation. *Biochim. Biophys. Acta* **1410**, 1-6.
- Nield J, Kruse O, Ruprecht J, da Fonesca P, Büchel C, Barber J (2000) 3D structure of *Chlamydomonas reinhardtii* and *Synechococcus elongatus* photosystem II complexes allow for comparison of their OEC organization. *J. Biol. Chem.* **275**, 27940-27946.

- Rhee K-H, Morris EP, Barber J, Kühlbrandt W (1998) Three dimensional structure of photosystem II reaction center at 8 Å resolution. *Nature* **396**, 283-286.
- Schubert W-D, Klukas O, Saenger W, Witt HT, Fromme P, Krauß N (1998) A common ancestor for oxygenic and anoxygenic photosynthetic systems: A comparison based on the structural model of photosystem I. *J. Mol. Biol.* **280**, 297-314.
- van Mieghem FJE, Sato K, Rutherford AW (1991) A chlorophyll tilted 30° relative to the membrane in the photosystem II reaction center. *Biochim. Biophys. Acta* **1058**, 379-385.
- Witt HT (1996) Primary reactions of oxygenic photosynthesis. *Ber. Bunsenges. Phys. Chem.* **100**, 1923-1942.
- Zouni A, Jordan R, Schlodder E, Fromme P, Witt HT (2000) First photosystem II crystals capable of water oxidation. *Biochim. Biophys. Acta* **1457**, 103-105.
- Zouni A, Lüneberg C, Fromme P, Schubert WD, Saenger W, Witt HT (1998) Characterization of single crystals of photosystem II from the thermophilic cyanobacterium *Synechococcus elongatus*. In: *Photosynthesis: Mechanisms and Effects* (ed. Garab, G.) Kluwer Academic Publishers, Dordrecht, pp. 925-928.
- Zouni A, Witt HT, Kern J, Fromme P, Krauß N, Saenger W, Orth P (2001) Crystal structure of photosystem II from *Synechococcus elongatus* at 3.8 Å resolution. *Nature* **409**, 739-743.